

NUMERICAL MODELLING OF COMPRESSIBLE INVISCID AND VISCOUS FLOW IN TURBINE CASCADES *

PETR LOUDA[†], KAREL KOZEL[‡], AND JAROMÍR PŘÍHODA[§]

Abstract. Mathematical models for inviscid and also viscous transonic flows through turbine cascades are presented. For numerical solution, finite volume upwind explicit (Runge-Kutta) and implicit (backward Euler) methods are considered. The flux splitting methods include AUSM, AUSMPW+ and HLLC Riemann solvers. The mathematical models are applied to flow through VKI and SE1050 turbine cascades.

Key words. implicit scheme, AUSM scheme, HLLC scheme

AMS subject classifications. 76H05, 76M12

1. Introduction. In this work some shock capturing upwind methods are used to solve compressible subsonic and transonic flow through 2D axial turbine cascades. The problems are formulated either for inviscid case or viscous case with the two-equation k - ω turbulence model. The formulation of boundary conditions allows subsonic inflow and outflow Mach numbers.

Several upwind flux splitting schemes are tested and compared in terms of quality of the results and CPU time requirement, by using explicit scheme in time and inviscid problem. For turbulent case and implicit scheme the CPU cost of the upwinding is less critical and easy linearization and extensibility to 3D problems is important. The simulated cases include subsonic and transonic flows through VKI and SE1050 turbine cascades. The results are compared also with available experimental data.

2. Mathematical models. The model for inviscid flow is based on Euler equations in Cartesian coordinates

$$\int_V \frac{\partial W}{\partial t} dV + \oint_{\partial V} F^I dS = 0, \quad (2.1)$$
$$W = \begin{bmatrix} \rho \\ \rho u_1 \\ \rho u_2 \\ \rho E \end{bmatrix}, \quad F^I = u_c \begin{bmatrix} \rho \\ \rho u_1 \\ \rho u_2 \\ \rho H \end{bmatrix} + \begin{bmatrix} 0 \\ p n_1 \\ p n_2 \\ 0 \end{bmatrix}$$

where V is control volume, n_i outer unit normal vector of its surface, t time, ρ density, u_i velocity vector, E total energy per unit volume, $H = E + p/\rho$ is total enthalpy and p static pressure. The magnitude of normal velocity $u_c = u_i n_i$. Equation of state for perfect gas is prescribed

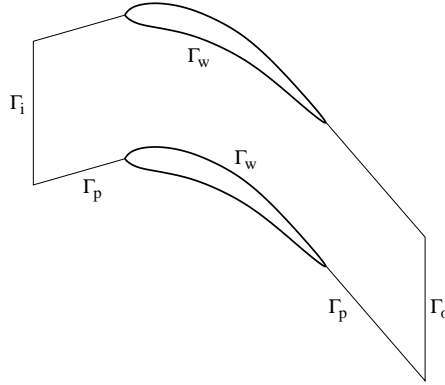
$$E = \frac{1}{\gamma - 1} \frac{p}{\rho} + \frac{1}{2} (u_1^2 + u_2^2), \quad (2.2)$$

*This work was supported by Grant of GA CR No.: P101/10/1329, P101/12/1271 and 201/08/0012.

[†]Dept. of Technical Mathematics, Czech Technical University in Prague, Karlovo nám. 13, CZ-121 35 Praha 2 (petr.louda@fs.cvut.cz).

[‡]Dept. of Technical Mathematics, Czech Technical University in Prague, Karlovo nám. 13, CZ-121 35 Praha 2

[§]Institute of Thermomechanics AS CR, Dolejškova 5, CZ-182 00 Praha 8

FIG. 2.1. *Solution domain*

with the ratio of specific heats $\gamma = 1.4$. The typical solution domain for 1 period of turbine cascade is shown in Fig. 2.1. For subsonic Mach numbers computed from velocity component normal to the boundary, 3 boundary conditions are to be prescribed on the inlet boundary Γ_i and 1 condition on the outlet boundary Γ_o .

Γ_i : inlet: prescribed inlet flow angle α_1 , total density ρ_0 and total static pressure p_0 .

Γ_o : outlet: prescribed mean value of static pressure p_2 (non-reflecting condition) according to the given outlet isentropic Mach number M_{2is} :

$$\frac{\int_{\Gamma_o} p dS}{\int_{\Gamma_o} dS} = p_2, \quad p_2 \left(1 + \frac{\gamma - 1}{2} M_{2is}^2 \right)^{\frac{\gamma}{\gamma - 1}} = p_0 \quad (2.3)$$

Γ_w : wall: normal velocity component $u_i n_i = 0$

Γ_p : periodic boundary: $W(t, r_i + P_i) = W(t, r_i)$, where P_i is periodicity of the cascade.

Further, mathematical model for turbulent flow is considered. It includes laminar diffusion as well as turbulent transport phenomena. The model is based on Favre-averaged Navier-Stokes (NS) equations, see e.g. Wilcox [11]. The system of averaged NS equations is then

$$\int_V \frac{\partial W}{\partial t} + \oint_{\partial V} F^I dS = \oint_{\partial V} F^V dS \quad (2.4)$$

$$F^V = \begin{bmatrix} 0 \\ t_{i1} + \tau_{i1} \\ t_{i2} + \tau_{i2} \\ (t_{ij} + \tau_{ij})u_j - q_i - q_i^t + d_i^t \end{bmatrix} n_i \quad (2.5)$$

where W , F^I have the same form as in Eq.(2.1). The molecular stress tensor and heat flux vector respectively are assumed in the form

$$t_{ij} = \mu 2S_{ij}, \quad S_{ij} = \frac{1}{2} \left(\frac{\partial u_i}{\partial x_j} + \frac{\partial u_j}{\partial x_i} \right) - \frac{2}{3} \delta_{ij} \frac{\partial u_k}{\partial x_k}, \quad (2.6)$$

$$q_i = -\frac{\gamma}{\gamma - 1} \frac{\mu}{Pr} \frac{\partial(p/\rho)}{\partial x_i}, \quad (2.7)$$

where δ_{ij} is Kronecker delta. The dynamic viscosity μ and Prandtl number

$$\mu = \text{const}, \quad Pr = \text{const}. \quad (2.8)$$

The total energy now includes the turbulent energy k

$$E = \frac{1}{\gamma - 1} \frac{p}{\rho} + \frac{1}{2}(u_1^2 + u_2^2) + k. \quad (2.9)$$

The effect of turbulent fluctuations is present by the Reynolds stress tensor τ_{ij} and turbulent heat flux q_i^t , which need to be modelled. An eddy viscosity model assumes

$$\tau_{ij} = \mu_t 2S_{ij} - \frac{2}{3} \delta_{ij} \rho k \quad (2.10)$$

$$q_i^t = q_i \frac{Pr}{\mu} \frac{\mu_t}{Pr_t} \quad (2.11)$$

where μ_t is eddy viscosity and the turbulent Prandtl number is set $Pr_t = 0.91$.

For turbulent scales, a two-equation model is solved. In the k - ω variant it can be written

$$\begin{aligned} \int_V \frac{\partial}{\partial t} \begin{bmatrix} \rho k \\ \rho \omega \end{bmatrix} dV + \oint_{\partial V} u_c \begin{bmatrix} \rho k \\ \rho \omega \end{bmatrix} dS = \oint_{\partial V} \begin{bmatrix} (\mu + \sigma_k \mu_T) \frac{\partial k}{\partial x_i} \\ (\mu + \sigma_\omega \mu_T) \frac{\partial \omega}{\partial x_i} \end{bmatrix} n_i dS + \\ + \int_V \begin{bmatrix} P_k - \beta^* \rho \omega k \\ \alpha \frac{\omega}{k} P_k - \beta \rho \omega^2 + CD \end{bmatrix} dV, \end{aligned} \quad (2.12)$$

where the turbulent production $P_k = \tau_{ij} \frac{\partial u_i}{\partial x_j}$, the α , β , β^* , σ_k , σ_ω are model coefficients and CD a cross-diffusion term. The eddy viscosity $\mu_t \sim k/\omega$. For used SST (Shear Stress Transport) model see Menter [9].

The boundary conditions for inviscid system are completed taking into account for diffusive terms and turbulence model equations:

Γ_i : prescribed α_1 , p_0 , ρ_0 and inlet local turbulence intensity I and inlet eddy viscosity μ_{t1} . Then

$$\frac{\partial T}{\partial n} = 0, \quad k = \frac{3}{2} I^2 (u_1^2 + u_2^2), \quad \omega = \rho k / \mu_{t1}, \quad (2.13)$$

where T is temperature. The value μ_{t1} has been chosen 10μ .

Γ_o : The outlet integral pressure (non-reflecting condition) p_2 is prescribed according to the given outlet isentropic Mach number M_{2is} . Further one requires

$$\frac{\partial T}{\partial n} = \frac{\partial k}{\partial n} = \frac{\partial \omega}{\partial n} = 0. \quad (2.14)$$

Γ_w : The blade surface is adiabatic and smooth. Then

$$u_1 = u_2 = \frac{\partial T}{\partial n} = k = 0, \quad \omega \sim \frac{\mu}{\rho y_{w1}^2}, \quad (2.15)$$

where y_{w1} is a sufficiently small measure comparable to viscous sublayer thickness.

Γ_p : periodic boundary: $W(t, r_i + P_i) = W(t, r_i)$, where P_i is periodicity of the cascade.

3. Numerical solution. The system of equations (2.4), (2.12) can be rewritten in the form

$$\frac{\partial}{\partial t} \int W d\mathcal{V} + \oint (F^I - F^V) d\mathcal{S} - \int Q d\mathcal{V} = 0, \quad (3.1)$$

where F^I , F^V , Q are inviscid flux, viscous flux and source terms respectively.

For spatial discretization we use a cell centered finite volume method with quadrilateral finite volumes (cells) denoted by indices i, j and composing a structured grid. The unknown $W_{i,j}$ is considered as cell-average value in the finite volume. The integrals in Eq. (3.1) are approximated using mid-point rule, leading to

$$\frac{dW_{i,j}}{dt} \Delta V_{i,j} + \text{Rez}(W)_{i,j} \Delta V_{i,j} = 0, \quad (3.2)$$

$$\text{Rez}(W)_{i,j} = \frac{1}{\Delta V_{i,j}} \sum_{\alpha=1}^4 (F_{\alpha}^I - F_{\alpha}^V)_{i,j} \Delta S_{i,j,\alpha} - Q_{i,j}, \quad (3.3)$$

where $\Delta V_{i,j}$ is area of the cell, $\Delta S_{i,j,\alpha}$ length of its face.

The numerical inviscid flux F_{α}^I on the interface α is easily formulated in supersonic flow, by cell-average values of F^I from the upwind side of the interface. In subsonic cases, approximate solutions of the Riemann problem will be used. The AUSM (Advection Upstream Splitting Method) flux vector splitting [6, 7] treats convective and acoustic (pressure) terms separately.

$$F_{1/2}^I = u_{c1/2} \begin{bmatrix} \rho \\ \rho u_1 \\ \rho u_2 \\ \rho H \\ \rho k \\ \rho \omega \end{bmatrix}_{L/R} + p_{1/2} \begin{bmatrix} 0 \\ n_1 \\ n_2 \\ 0 \\ 0 \\ 0 \end{bmatrix}, \quad [\cdot]_{L/R} = \begin{cases} [\cdot]_L & \text{for } u_{c1/2} \geq 0, \\ [\cdot]_R & \text{otherwise,} \end{cases} \quad (3.4)$$

where L , R denote states on the left and right hand side of the interface $1/2$ and $u_{c1/2}$, $p_{1/2}$ are suitably defined interface velocity and pressure depending on Mach number. Nevertheless, to diminish possible wiggles of pressure, pressure weighted formulations of $u_{c1/2}$ were later developed. In this work the AUSMPW+ variant [4] is also used.

The other approximate solution of Riemann problem assumes 3 wave speeds and leads to the HLLC flux proposed by Toro et al [10] who extended Harten-Lax-van Leer (HLL) flux based on only 2 acoustic waves by contact discontinuity solution. The formulation was further refined by Batten et al [2].

The L , R states on the left or right from the interface considered are needed in all upwind methods. Taking cell-averages in the finite volumes adjacent to the interface, first order accuracy method is obtained. For higher accuracy needed for turbulent flow computations, the linear extrapolation for conservative variables with limiter was applied. Considering e.g. the face $i + 1/2$ between cells (i, j) and $(i + 1, j)$ we have

$$\begin{aligned} W_L &= W_{i,j} + \frac{1}{2} \Psi(r_L) \Delta^-, & W_R &= W_{i+1,j} - \frac{1}{2} \Psi(r_R) \Delta^+, \\ \Psi(r) &= \frac{r + |r|}{|r| + 1}, & r_L &= \frac{\Delta + \epsilon}{\Delta^- + \epsilon}, & r_R &= \frac{\Delta + \epsilon}{\Delta^+ + \epsilon}, & \epsilon &= 10^{-17}, \\ \Delta^- &= W_i - W_{i-1}, & \Delta &= W_{i+1} - W_i, & \Delta^+ &= W_{i+2} - W_{i+1}, \end{aligned} \quad (3.5)$$

where Ψ is the van Leer limiter, switching to first order upwind at occurrence of a local extremum of W (adjacent slopes Δ have opposite sign).

The discretization of diffusive flux is central. The approximation of cell face derivatives needed in diffusive terms uses quadrilateral dual finite volumes constructed over each face of primary volume – the vertices are located at end of primary face and in centres of adjacent primary volumes. The mid-point rule quadrature formula is again used, with face value of velocity defined as average of values in vertices of dual cell [8].

For time discretization, the explicit Runge-Kutta method and the backward Euler scheme (implicit) were used. The multi-stage Runge-Kutta method can be written

$$W_{i,j}^{(0)} = W_{i,j}^n \tag{3.6}$$

$$W_{i,j}^{(l)} = W_{i,j}^{(l-1)} - \alpha_{(l)} \Delta t Rez(W^{(l-1)})_{i,j} \tag{3.7}$$

$$W_{i,j}^{n+1} = W_{i,j}^{(m)}, \quad (l = 1, \dots, m), \tag{3.8}$$

For e.g. 3-stage scheme the $\alpha_1 = \alpha_2 = 1/2, \alpha_3 = 1$.

The backward Euler scheme can be written

$$\frac{W_{i,j}^{n+1} - W_{i,j}^n}{\Delta t} = Rez(W^{n+1})_{i,j} \tag{3.9}$$

where the steady residual at new time level is approximated by linear extrapolation

$$Rez(W^{n+1})_{i,j} = Rez(W^n)_{i,j} + \sum_{\alpha \in S} \frac{\partial Rez(W^n)_{i,j}}{\partial W_\alpha} (W_\alpha^{n+1} - W_\alpha^n) \tag{3.10}$$

The Jacobi matrices $\partial Rez(W^n)_{i,j} / \partial W_\alpha$ are obtained as derivatives of discrete expression for Rez with respect to nodal values W_α from the stencil S of implicit operator. We chose

$$S = \{ (i, j), (i - 1, j), (i + 1, j), (i, j - 1), (i, j + 1) \} \tag{3.11}$$

which leads to block 5-diagonal system of linear equations. The system is solved iteratively by a block relaxation method with direct block tri-diagonal solver on selected family of grid lines. Note that the extension of the method to 3D is straightforward and indeed has been done. Numerical solutions of some 3D cases of incompressible flow are given in [8].

4. Numerical results. The model of inviscid flow is applied to the MUR43 test case of the VKI turbine cascade [1]. The outlet Mach number is $M_{2is} = 0.84$ and the flow is almost completely subsonic. The results are scaled by chord length and p_0 and ρ_0 . In the table 4.1, computational times for different upwind schemes are compared. The time scheme is Runge-Kutta, thus the computation of upwind flux takes most time and total CPU time can represent the CPU demand of an upwind flux. As can be seen, the HLLC scheme requires considerably more CPU time than the simplest AUSM scheme. However, in viscous flow, the difference becomes much smaller and in implicit schemes the linear solver consumes most of the time. For implicit method, we prefer AUSM or AUSMPW+ over HLLC for easier linearization.

The convergence history for inviscid MUR43 is shown in Fig. 4.1 in the form of L_2 norm of steady residual of total energy E . The convergence is not particularly good

TABLE 4.1
Relative CPU times for different upwind schemes, Runge-Kutta method in time

| AUSM | AUSMPW+ | HLLC |
|------|---------|------|
| 1 | 1.20 | 1.36 |

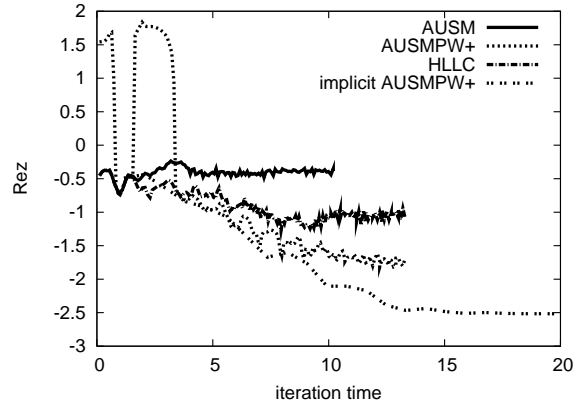


FIG. 4.1. Convergence histories for inviscid MUR43 case

for either method, however is best for AUSMPW+ explicit and implicit schemes. The corresponding number of time steps is 40000 for Runge-Kutta method and 2000 for implicit method.

The next Fig. 4.2 compares pressure on the blade with measurement. All more diffusive schemes (AUSMPW+, HLLC) give same results, less diffusive AUSM is slightly different on a part of suction side, where the deviation from measurement is largest. This suggests an influence of boundary layer not captured in the numerical simulation.

The Fig. 4.3 shows isolines of Mach number for inviscid MUR43 case and 3 methods. The results are very similar.

The qualitative errors of a numerical method can be observed on enthalpy–entropy diagram of the cascade. For the above results it is shown in Fig. 4.4. The enthalpy h and entropy s are defined respectively

$$h = H - \frac{1}{2}(u_1^2 + u_2^2), \quad s = c_v \ln \left(\frac{1}{r} \frac{p}{\rho^\gamma} \right), \quad (4.1)$$

where c_v is specific heat at constant volume and r gas constant. Since the simulation does not explicitly depend on c_v and r , they are set to 1 for the purpose of h – s diagram. The values Eq. (4.1) are computed locally over 1 period of the cascade, for 20 uniformly distributed cuts $x = \text{const}$. In the Fig. 4.4 one can see for AUSM scheme wiggles on both ends of the graph, which correspond to regions near the inlet and the outlet boundary. The unphysical decrease of entropy is then caused by boundary conditions interacting with the numerical method. The enthalpy decreases from leading edge to the trailing edge, otherwise is approximately constant. The entropy is constant up to the leading edge, then starts to slowly increase. However, for all methods except for AUSM there is slight decrease of entropy approximately for $0.25 < x/c < 0.40$, which is error of the simulation and correlates with the largest

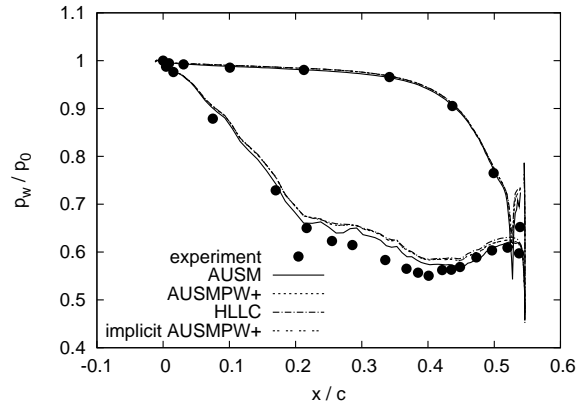


FIG. 4.2. Pressure on the blade for inviscid MUR43 case

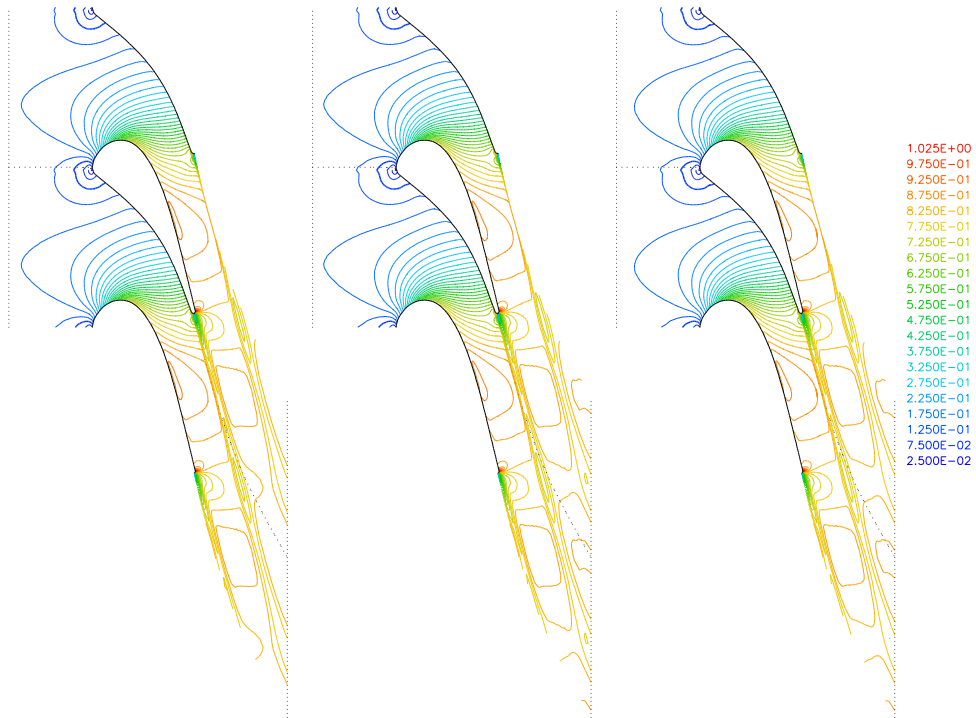


FIG. 4.3. Isolines of Mach number for inviscid MUR43 case. From left to right: Runge-Kutta HLLC method, Runge-Kutta AUSMPW+ method, implicit AUSMPW+ method

difference vs. measurement, see Fig. 4.2. The cause of this error might be the inviscid model in the first place. There is large jump in entropy near the trailing edge, where the numerical viscosity of the method plays a role.

Next we consider flow through the SE1050 turbine cascade [13, 12]. Four regimes with sonic to supersonic outlet Mach number are considered. The $M_{2is} = \{1.007, 1.100, 1.198, 1.313\}$, the inlet angle $\alpha_1 = 19.3^\circ$ and inlet turbulence intensity was

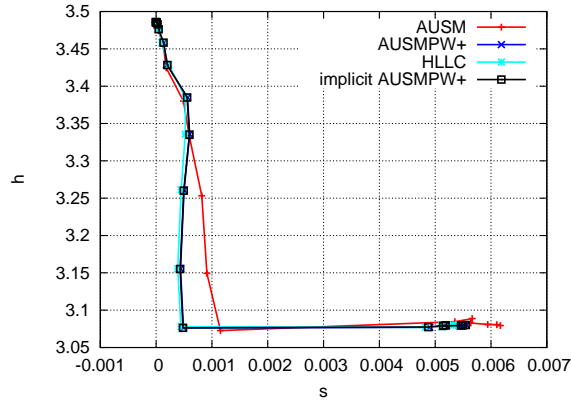


FIG. 4.4. Enthalpy–entropy diagram of the MUR43 case

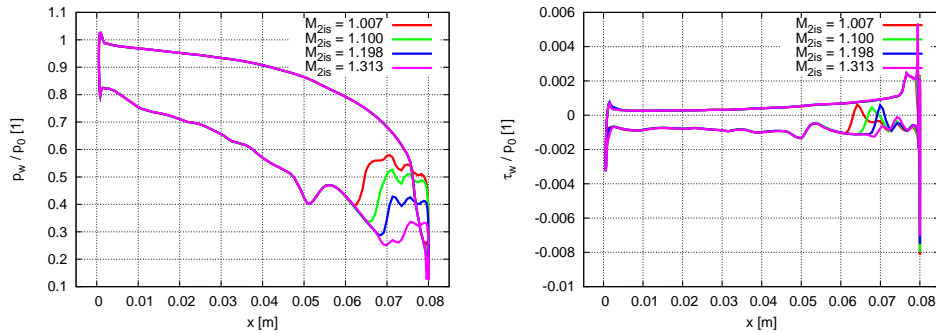


FIG. 4.5. Pressure and friction on the blade surface, SE1050 cascade

estimated $I = 2\%$.

The finite volume grid is of multiblock type with O-grid around blade and H-type grid in the remaining domain, consisting of approx. 22 500 finite volumes and refined near the blade. The problem is solved by the implicit AUSMPW+ method with the van Leer limiter.

The transonic case with $M_{2is} = 1.198$ was compared by authors with experimental results in terms of static pressure on the blade and isolines of Mach number in the paper [5]. The results compare well also with laminar results of several different schemes [3].

The pressure and friction on the blade for all regimes are shown in Fig. 4.5. One can see the shock wave decreasing in intensity and moving towards trailing edge with increasing Mach number. The isolines of Mach number for all regimes are shown in Fig. 4.6. Finally the enthalpy–entropy diagram is shown in Fig. 4.7. There is no unphysical phenomenon except for very slight decrease of entropy in the vicinity of the leading edge.

5. Conclusions. Mathematical models for inviscid and also turbulent compressible flow through 2D turbine axial cascades with subsonic inlet were presented. The numerical solution of the models, based on cell-centered finite volume discretization was shown in the form of explicit Runge-Kutta method and implicit Euler method

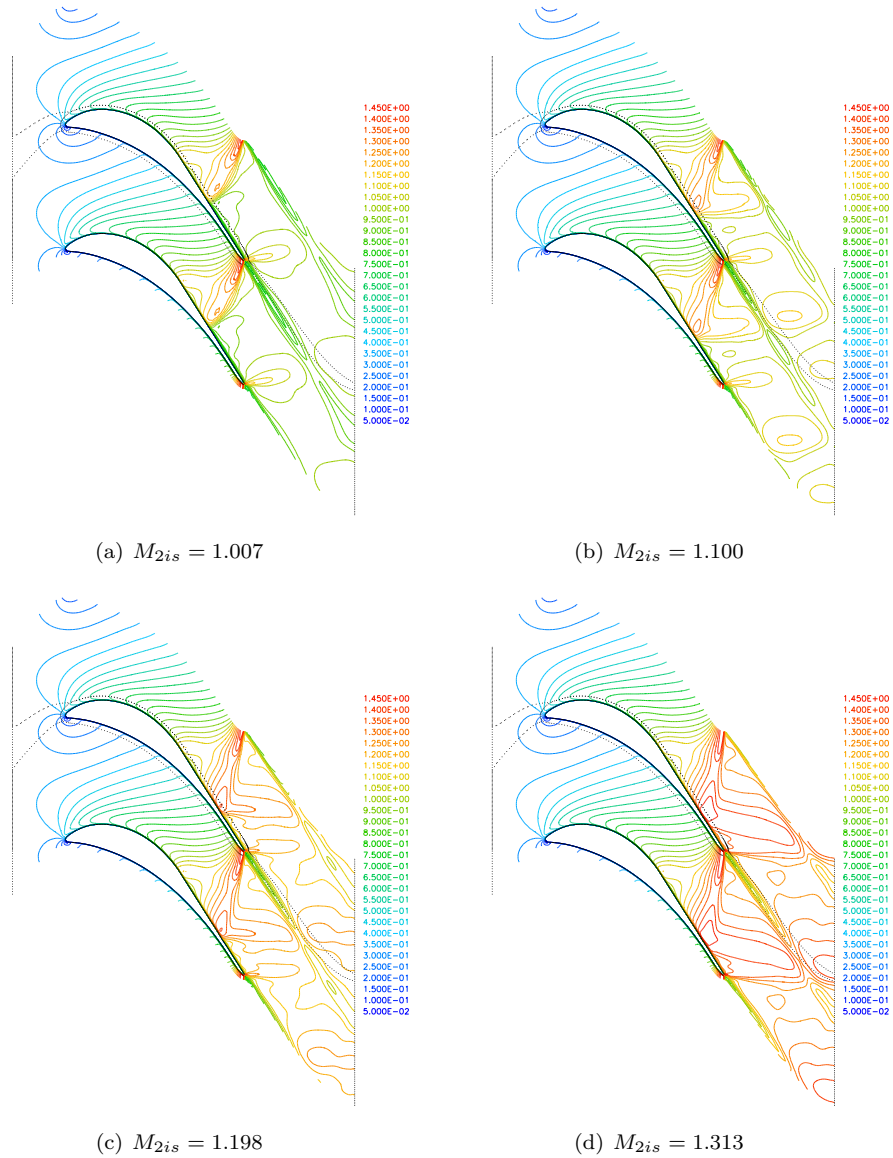


FIG. 4.6. Isolines of Mach number for different outlet Mach numbers, SE1050 cascade

considering AUSM and HLLC flux splitting. The results were obtained for VKI and SE1050 turbine cascades. The physical correctness of the results was observed by means of enthalpy–entropy diagram. Some minor violation of second law of thermodynamics has been observed and shown to correlate with deviation from measurement. For turbulent simulations, the implicit discretization is necessary and AUSMPW+ flux splitting provides acceptable accuracy, robustness and computational cost.

Acknowledgments. This work was supported by the grants of GA CR No. P101/10/1329,P101/12/1271 and 201/08/0012.

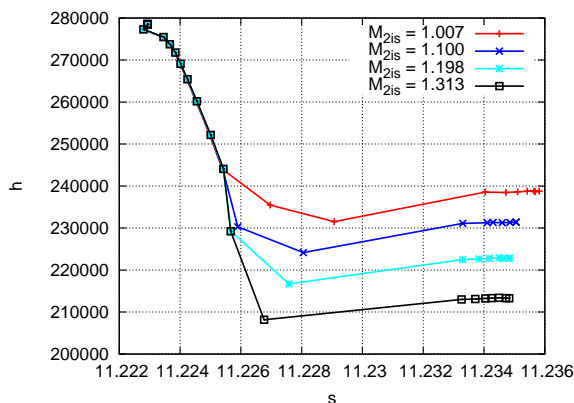


FIG. 4.7. Enthalpy–entropy diagram of the SE1050 case

REFERENCES

- [1] T. Arts, M. Lambert de Rouvroit, and A. W. Rutherford. Aerothermal investigation of a highly loaded transonic linear turbine guide vane cascade. Technical report, von Karman Institute, 1990. VKI Technical Note 174.
- [2] P. Batten, N. Clarke, C. Lambert, and D. M. Causon. On the choice of wavespeeds for the HLLC Riemann solver. *SIAM J. Sci. Comput.*, 18(6):1553–1570, November 1997.
- [3] Dobeš J., Fořt J., Fürst J., Halama J., and Kozel K. Numerical solution of transonic flows in 2D and 3D axial and radial turbine cascades. In *5th European conference on turbomachinery*, pages 1105–1114, Prague, 2003.
- [4] K. H. Kim, C. Kim, and O.-H. Rho. Methods for accurate computations of hypersonic flows I. AUSMPW+ scheme. *J. of Computational Physics*, 174:38–80, 2001.
- [5] K. Kozel, P. Louda, and J. Příhoda. Numerical modeling of turbulent flows in turbine cascades. In *4th International Conference on Advanced Computational Methods in Engineering*, Liège, 2008. CD-ROM.
- [6] M.-S. Liou. On a new class of flux splittings. *Lecture Notes in Phys.*, 414:115–119, 1993.
- [7] M.-S. Liou and C. J. Steffen. A new flux splitting scheme. *J. Computational Physics*, 107:23–39, 1993.
- [8] P. Louda. *Numerical solution of 2D and 3D turbulent impinging jet flow*. PhD thesis, FME CTU, Prague, 2002. (in Czech).
- [9] F. R. Menter. Two-equation eddy-viscosity turbulence models for engineering applications. *AIAA Journal*, 32(8):1598–1605, 1994.
- [10] E. F. Toro, M. Spruce, and W. Speares. Restoration of the contact surface in the HLL-Riemann solver. *Shock Waves*, 4:25–34, 1994.
- [11] D. C. Wilcox. *Turbulence modeling for CFD*. DCW Industries, Inc., California, 1998. 2nd edition.
- [12] P. Šafařík, M. Štastný, and M. Babák. Numerical and experimental testing of transonic flow in the etalon turbine cascade SE 1050. In G. Bois M. Štastný, C. H. Sieverding, editor, *5th European Conference on Turbomachinery*. Czech Technical University in Prague, 2004.
- [13] M. Štastný and P. Šafařík. Experimental analysis data on the transonic flow past the plain turbine cascade. Technical report, 1990. Paper 90-GT-313.